<< Previous Chapter

Chapter 10

Inverse Methods

All of the previous chapters have been concerned with the *forward* or *direct problem of hydrologic optics*. The rules of the game were simple: *given the inherent optical properties of the water and the physical properties of the boundaries, find the radiance distribution throughout the water.* The development of the governing equations in the first five chapters, the discussions of numerical solution methods in the previous four chapters, and the example solutions yet to come in Chapter 11 convince us that we can readily compute radiance distributions in natural waters. Indeed, the only limits on the accuracy of computed radiances are the accuracy with which we specify the IOP's and the boundary conditions, and the amount of computer time we wish to devote to the numerical solutions. In this sense *the direct problem of computing radiances can be regarded as solved.*

We now turn our attention to *the inverse problem of hydrologic optics: given radiometric measurements of underwater light fields, determine the inherent optical properties of the water.* We shall soon learn that this is very much an *unsolved problem.* Both conceptual and practical limits are encountered in inverse problems.

10.1 Inverse Problems

The first problem we encounter is *uniqueness of the solution*. Consider the following situation. A body of water with a particular set of IOP's and certain boundary conditions has an underwater radiance distribution $L_1(z;\theta,\phi;\lambda)$. If the boundary conditions now change, perhaps because the wind ruffles the sea surface or the sun moves, there will be a different radiance distribution $L_2(z;\theta,\phi;\lambda)$ within the water, even though the IOP's remain unchanged. Can we correctly recover the same set of IOP's from the two different light fields? Can we distinguish between $L_1 \neq L_2$ because of a change in boundary conditions, as opposed to $L_1 \neq L_2$ because of a change in IOP's? If the same set of IOP's can yield different radiance distributions, as we just saw, we are led to ask if two different sets of IOP's and boundary conditions can lead to the same radiance distribution. In other words, *is there even in principle a unique solution to the inverse problem stated above*?

Another problem often encountered with inverse solutions is the *stability of the solution*, or its *sensitivity to errors in the measured radiometric variables.* In direct problems we usually find that a small error (say 5%) in the IOP's leads to a correspondingly small error in the computed radiance. With inverse problems we often find that small errors in the measured radiometric quantities lead to large errors, or even unphysical results, in the retrieved IOP's. Such extreme sensitivity of the inversion scheme to small errors in the input data often renders inversion algorithms useless, even though they appear in principle to be quite elegant and satisfactory.

From a practical standpoint, if we have to measure the entire radiance distribution throughout the water body (perhaps with high accuracy), we probably could measure the IOP's themselves just as easily. An inverse method is useful only when it saves us time, money, or effort. What would be of real value is a recovery of the IOP's from, say, easily measured irradiances. We already have seen one example of this in Gershun's law, Eq. (5.37), which (in principle, at least) allows us to recover the absorption coefficient a from measured values of the plane and scalar irradiances, if there are no internal sources present. We thus ask, for example, what additional measurements must be made in order to recover both the absorption and the scattering coefficients, a and b, or perhaps both a and $\beta(\psi)$. It is problems like this to which we now turn our attention.

Classification of inverse problems

There are many kinds of inverse problems. For example, there are *medium characterization problems*, for which the goal is to obtain information about the IOP's of the medium, which in our case is the water body with all of its constituents. This is the type of problem that we consider in this chapter. There are also *hidden-object characterization problems*, for which the goal is to detect or obtain information about an object imbedded within the medium, for example a submerged submarine. We shall not discuss this type of problem. Inverse problems may use optical measurements made *in situ*; such problems are discussed in Sections 10.2-10.4. *Remote sensing* uses measurements made outside the medium, typically from a satellite or aircraft. We discuss remote sensing in Section 10.5.

Another type of inverse problem seeks to determine the properties of individual particles from light scattered by *single* particles. In such problems we usually start with considerable knowledge about the particles (for example, the particles are spherical and have a known radius), and we

seek to determine another specific bit of information (such as the particle index of refraction). The associated inversion algorithms usually assume that the detected light has been singly scattered. Even these highly constrained problems can be very difficult.

Many researchers are actively addressing such problems because of their frequent occurrence in science and industry. We shall not discuss these "individual-particle" inverse problems. The state of the art can be seen in a recent special issue of *Applied Optics* (Hirleman and Bohren, 1991). In the ocean, there is no escaping multiple scattering, which greatly complicates the problem.

The solutions to inverse problems fall into two categories: explicit and implicit. *Explicit solutions* are formulas that give the desired IOP's as functions of measured radiometric quantities. The simplest example is Gershun's law when solved for the absorption in terms of the irradiances. Such solutions are rare. *Implicit solutions* are obtained by *solving a sequence of direct problems*. In crude form, we can imaging having a measured radiance distribution. We then solve direct problems to predict the radiance for each of many different sets of IOP's. Each predicted radiance is compared with the measured radiance. The IOP's associated with the predicted radiance that most closely matches the measured radiance are then taken to be the solution of the inverse problem. We shall see a simple example of this process in Section 11.1. Such a plan of attack can be efficient if we have a rational way of changing the IOP's from one direct solution to the next, so that the sequence of direct radiance solutions converges to the measured radiance. We shall see examples of both solution categories below.

The classification of inverse problems is discussed in detail in the review paper by McCormick (1992b).

10.2 Inversion of the RTE

Let us recall the integral Eq. (9.87) relating the asymptotic radiance distribution $L_\infty(\mu)$ to the IOP's ω_o and $\tilde{\beta}$.

$$(1 - \kappa_\infty \mu)\, L_\infty(\mu) = \omega_o \int\!\!\int_{\Xi'} L_\infty(\mu')\, \tilde{\beta}(\mu',\phi' \to \mu,\phi)\, d\mu'\, d\phi' . \qquad (10.1)$$

In Chapter 9 we presumed to know the IOP's, and we regarded this equation as one to be solved for κ_∞ and $L_\infty(\mu)$. We can just as well imagine determining $L_\infty(\mu)$ and κ_∞ by measurements at great optical depth, and then

solving Eq. (10.1) for ω_o and $\tilde{\beta}$. However, use of this equation requires us to be in homogeneous water, so that an asymptotic radiance distribution exists. In addition, we must make our measurements within the asymptotic regime, i.e. at great depth. These two requirements rule out the use of Eq. (10.1) near the surface or for inhomogeneous waters, which are precisely the situations of greatest interest in hydrologic optics.

Uniqueness of the inversion

Let us suppose that we have measured the radiance distribution $L(z;\theta,\phi)$ throughout a water body. We then azimuthally average $L(z;\theta,\phi)$ to get

$$L(z;\theta) \equiv \frac{1}{2\pi}\int_0^{2\pi} L(z;\theta,\phi)\, d\phi \,.$$

Zaneveld (1974) expanded $L(z;\theta)$ and the volume scattering function (VSF) β as series of Legendre polynomials:

$$\begin{aligned} L(z;\theta) &= \sum_{n=o}^{\infty} A_n(z)\, P_n(\cos\theta) \\ \beta(\psi) &= \sum_{n=o}^{\infty} B_n\, P_n(\cos\psi)\,. \end{aligned} \tag{10.2}$$

Substituting the forms (10.2) into the azimuthally averaged, source-free RTE led to a set of differential equations for the expansion coefficients A_n and B_n. These equations eventually led to explicit formulas for the beam attenuation coefficient c,

$$c = \lim_{n\to\infty}\left\{ -\frac{\displaystyle\int_0^{\pi} \frac{dL(z;\theta)}{dz}\, P_n(\cos\theta)\cos\theta\sin\theta\, d\theta}{\displaystyle\int_0^{\pi} L(z;\theta)\, P_n(\cos\theta)\sin\theta\, d\theta} \right\}, \tag{10.3}$$

and for the VSF,

$$\beta(\psi) = \sum_{n=0}^{\infty} \frac{2n+1}{4\pi} P_n(\cos\psi) \left[c + \frac{\displaystyle\int_0^{\pi} \frac{dL(z;\theta)}{dz}\, P_n(\cos\theta)\cos\theta\sin\theta\, d\theta}{\displaystyle\int_0^{\pi} L(z;\theta)\, P_n(\cos\theta)\sin\theta\, d\theta} \right] \tag{10.4}$$

Equations (10.3) and (10.4) give us a very important result: *The radiance and its depth derivative together uniquely determine the IOP's c and* β. We can thus lay to rest our philosophical (but not our practical) concerns about the uniqueness of IOP's associated with a particular light field. Note, however, that having $L(z;\theta,\phi)$ at only one depth is not sufficient to uniquely specify the IOP's at that depth. We must also know *dL/dz*, which can be estimated from measurements at two closely spaced depths.

Unfortunately, though, Eqs. (10.3) and (10.4) are of little use for actual retrievals of *c* and β from measured radiances. The reason becomes clear if we recall from Fig. 9.1 that an expansion of natural-water phase functions in Legendre polynomials, as in Eq. (10.2), requires hundreds of terms. We must have the same number of terms in Eq. (10.4). Computing the high-order B_n coefficients requires that *L* and *dL/dz* be measured with extreme accuracy and directional resolution in order to evaluate the integrals seen in Eq. (10.4). In practice, we can at best measure L to an accuracy of a few percent on a θ-grid with a resolution of a few degrees. This is by no means sufficient for a retrieval of β. Similarly, we note in Eq. (10.3) that *c* is obtained from the limit of an infinite sequence of terms like those involved with β.

McCormick (1986) has reviewed the large body of literature on inversion algorithms based on expansions of *L* and $\tilde{\beta}$ in fashions similar to Eq. (10.2), but including the φ dependence of $L(z;\theta,\phi)$. Many of these algorithms rely on the additional information contained in the azimuthal dependence of the radiance. These algorithms may work in situations where Rayleigh or isotropic scattering is applicable, so that only a few terms in the $\tilde{\beta}$ expansion are required. Such situations occur, for example, in atmospheric optics and in neutron diffusion, but not in natural waters. However, these algorithms suffer the same inability to handle highly peaked phase functions as does Zaneveld's method.

The Wells compound radiometer **See Note**

Wells (1983) performed a decomposition of *L* and β similar to that seen in Eq. (10.2) [see Supplemental Note 12]. He defined moments of the radiance distribution as

$$L_n(z) \equiv 2\pi \int_0^{\pi} L(z;\theta)\, P_n(\cos\theta)\, \sin\theta\, d\theta\,,$$

where $L(z;\theta)$ is the azimuthally averaged radiance and n = 0, 1, 2, ... Likewise, the moments S_n of the volume scattering function β are defined

by

$$S_n \equiv 2\pi \int_0^{\pi} \beta(\psi)\, P_n(\cos\psi)\, \sin\psi\, d\psi\,. \tag{10.5}$$

A related set of coefficients D_n [which Wells denoted by A_n, but which must not be confused with the A_n of Eq. (10.2)] is defined by

$$D_n \equiv c - S_n\,,$$

where c is the beam attenuation coefficient. Note from Eq. (10.5) that $S_0 = b$ and that $S_\infty = 0$ (from the nature of P_n as $n \to \infty$); hence, $D_0 = a$ and $D_\infty = c$. The D_n are IOP's, and knowing them is equivalent to knowing a, c, and β. Physically, the D_n can be loosely interpreted as decay rates with depth for the L_n.

Wells showed that the D_n are determined from the moments of the radiance via

$$D_n = -\frac{n\,\dfrac{dL_{n-1}}{dz} + (n+1)\,\dfrac{dL_{n+1}}{dz}}{(2n+1)\,L_n}\,, \tag{10.6}$$

where $L_{-1} \equiv 0$. Note that Eq. (10.6) for $n = 0$ is just Gershun's law.

Wells realized that the radiance moments L_n can be *measured directly* by an instrument whose angular response is proportional to $P_n(\cos\theta)$ and independent of ϕ. Such an instrument has been constructed (Doss and Wells, 1992). The prototype instrument uses ten specially shaped mirrors to measure L_0, ..., L_9, from which D_0, ..., D_8 are computed by Eq. (10.6). The needed derivatives of L_n are estimated from measurements of L_n at closely spaced depths. The instrument thus gives the first nine terms of the D_n sequence. An independent measurement of c, which is easily made, gives D_∞. One can then estimate the remaining D_n, $n \geq 9$, by interpolation based on D_0, ..., D_8 and D_∞. The VSF is then recovered by inverting Eq. (10.5) to get

$$\beta(\psi) = \sum_{n=0}^{\infty} \frac{2n+1}{4\pi}\,(c - D_n)\,P_n(\cos\psi)\,.$$

Note that this equation in essentially the same as Eq. (10.4).

The initial sea trial of this instrument (Doss and Wells, 1992) showed a good recovery of the total absorption coefficient $a = D_0$ when compared to a values determined by filter-pad techniques. It should be noted that the instrument gives an *in-situ, real-time* determination of the absorption. The recovered $\beta(\psi)$ looked realistic *except* at $\psi > 160°$. The

unrealistic behavior of β for large ψ was probably due to inaccurate estimation of the D_n's for large n values. No instrument was available for a direct measurement of $\beta(\psi)$.

10.3 Inversions Based on the Irradiance Quartet

We have just seen that inverting the RTE given measured radiances is in principle possible, but is in practice a difficult-to-impossible task. We now investigate what information can be recovered from measured irradiances. In this section we assume that downwelling and upwelling plane and scalar irradiances are measured as functions of depth z at the wavelength of interest. These quantities form the *irradiance quartet*

$$[\, E_d(z),\ E_u(z),\ E_{od}(z),\ E_{ou}(z)\,] .$$

Because these irradiances contain less information than the radiance, we expect to recover less information than can in principle be obtained by inverting the RTE. But since the governing two-flow equations have a simpler mathematical form than the integro-differential RTE, they may yield more easily to inversion. We first consider formal inversions of the two-flow and related equations. We then consider other ways to squeeze information from the irradiance quartet.

Information requirements for the inversion

We know from problem 5.1 that adding the two-flow equations yields Gershun's law, which then can be solved in source-free waters for the absorption coefficient a:

$$a(z) \;=\; -\,\frac{1}{E_{od}(z) + E_{ou}(z)}\,\frac{d}{dz}\big[\, E_d(z) - E_u(z)\,\big] .$$

This is the simplest possible inversion of the two-flow equations. Errors in the measured irradiances, or the presence of internal sources, will result in errors in the recovered absorption coefficient. At the end of Section 5.9, we cited recent applications of Gershun's law to the recovery of a.

Gershun's law gives us one equation in one unknown, and a measured irradiance quartet provides sufficient information to effect the inversion. The needed derivative can be estimated from measurements at different depths.

We next examine the two-flow Eqs. (5.54) and (5.55) from the information standpoint. These equations can be written to show the members of the irradiance quartet explicitly:

$$\frac{dE_d}{dz} = -\left(a \frac{E_{od}}{E_d} + b_{du} \right) E_d + b_{ud} E_u \tag{10.7}$$

$$-\frac{dE_u}{dz} = -\left(a \frac{E_{ou}}{E_u} + b_{ud} \right) E_u + b_{du} E_d . \tag{10.8}$$

We thus have two equations in the three unknowns a, b_{du} and b_{ud}, which is insufficient to obtain a unique inversion.

In order to proceed, we can follow either of two paths. First, we can conjure up a third independent equation relating the unknowns and the irradiance quartet, so that we have three equations in three unknowns. Or second, we can add an additional measurement (for example, an independent measurement of the absorption coefficient a) to the irradiance quartet, so that we have left only two unknowns.

The algorithm of Preisendorfer and Mobley

Preisendorfer and Mobley (1984) chose the first path, as follows. The different directional structures of the upwelling and downwelling radiance distributions cause b_{ud} to differ from b_{du}, as we saw in Section 5.10. Because these directional structures are parameterized in terms of the mean cosine $\bar{\mu}_u$ and $\bar{\mu}_d$, Preisendorfer and Mobley reasoned (incorrectly) that the differences in b_{ud} and b_{du} could to a large extent be removed by the mean cosines. They thus *assumed* that

$$b_{ud} \bar{\mu}_u = b_{du} \bar{\mu}_d \equiv \bar{b}_b . \tag{10.9}$$

Equation (10.9) is exact for isotropic scattering, in which case $\bar{b}_b = b_b$, the backscattering coefficient of Eq. (3.6b). It was hoped that Eq. (10.9) would remain a useful approximation for anisotropic phase functions, and $\bar{b}_b$ was termed a "mean backscattering coefficient." Note that $\bar{b}_b$ is an AOP, which was presumed to be roughly equal to the IOP b_b. As we saw in Section 5.12, recovery of a and b_b would be particularly valuable because these are the two IOP's most responsible for determining "ocean color," as manifested in the irradiance reflectance R [recall Eq. (5.75), for example].

Equation (10.9) provides the needed third equation for use along with Eqs. (10.7) and (10.8). Use of Eq. (10.9) then reduces the two-flow

equations to two equations in the two unknowns a and $\bar{b}_b$:

$$\frac{dE_d}{dz} = -(a + \bar{b}_b)\frac{1}{\bar{\mu}_d}E_d + \bar{b}_b\frac{1}{\bar{\mu}_u}E_u \tag{10.10}$$

$$-\frac{dE_u}{dz} = -(a + \bar{b}_b)\frac{1}{\bar{\mu}_u}E_u + \bar{b}_b\frac{1}{\bar{\mu}_d}E_d . \tag{10.11}$$

The mean cosines are of course computable from their definitions (3.14) and (3.15) if the irradiance quartet is measured.

Preisendorfer and Mobley went on to develop a rather complicated iterative inversion scheme for Eqs. (10.10) and (10.11), rather than just explicitly solving Eqs. (10.10) and (10.11) for a and $\bar{b}_b$ for each set of measured irradiances and estimated (by finite differences in depth) derivatives.

The purpose of their implicit solution scheme was the following. Suppose that the four members of the irradiance quartet are measured at discrete depths z_i. $i = 1, 2, ..., I$. *The iterative scheme then recovers depth profiles* $a(z)$ *and* $\bar{b}_b(z)$ *that exactly reproduce the measured irradiances* $E_d(z_i)$ and $E_u(z_i)$ when $a(z)$ and $\bar{b}_b(z)$ are used in Eqs. (10.10) and (10.11), and the equations are integrated with depth. The algorithm thus has *the desirable property of achieving an inversion that is consistent with the available data.*

Unfortunately, however, the fundamental assumption (10.9) leading to Eqs. (10.10) and (10.11) is flawed. Aas (1987) and later Stavn and Weidemann (1989) showed that for oceanic water, $b_{ud}\bar{\mu}_u$ is typically two to four times $b_{du}\bar{\mu}_d$. These authors introduced the *shape factors*

$$r_u \equiv \frac{b_{ud}\bar{\mu}_u}{b_b} \quad \text{and} \quad r_d \equiv \frac{b_{du}\bar{\mu}_d}{b_b} . \tag{10.12}$$

Assumption (10.9) is then equivalent to assuming that $r_u = r_d$. Numerical simulations by Stavn and Weidemann showed that the ratio r_u/r_d depends on the composition of the sea water, which is highly variable. Their results return us to a problem with two equations and three unknowns, which can be viewed as a, r_u, and r_d; or as a, b_b, and r_u/r_d. Extensive observational data or numerical simulations could perhaps reveal relationships between r_u, r_d and water composition, so that we could again reduce the inversion problem to two unknowns in two equations. However, this line of research has not been pursued.

In summary, the proper view of the Preisendorfer-Mobley inversion algorithm is that it recovers two numbers, a and $\overline{b}_b$, which when used in Eqs. (10.10) and (10.11) exactly reproduce the measured plane irradiances. However, it is not possible to relate the AOP $\overline{b}_b$ to the IOP b_b in any simple fashion. We include this discussion of the Preisendorfer-Mobley algorithm because its failure highlights *an inherent weakness in inversions based on the two-flow equations*, or upon any simplification thereof [such as the model developed in Stavn and Weidemann (1989)]. *The two-flow equations cannot be inverted without making an a priori assumption*, which usually is cast as an assumption about the diffuse backscatter coefficients b_{du} and b_{ud}. However, because of the variability of these quantities in natural waters, we have little guidance on how to formulate the needed assumption.

The algorithm of McCormick and Rinaldi

McCormick and Rinaldi (1989) developed an algorithm that recovers the *similarity parameter*

$$s = \left[1 + \frac{b}{a}(1 - g)\right]^{-1/2} \tag{10.13}$$

from measurements of the irradiance quartet at two depths. Here g is the mean cosine of the scattering phase function, defined as in Eq. (3.8b). The significance of s is that quantities such as the reflectance of a water body are nearly the same for water bodies having different a, b and g values, but having the same value of s. Similarity parameters are discussed in general by van de Hulst (1980, Chapter 14).

Let $E(z) \equiv E_d(z) - E_u(z)$ be the net irradiance defined in Eq. (1.28), and let

$$\Delta E^2(z_1,z_2) \equiv E^2(z_1) - E^2(z_2)$$
$$\Delta E_o^2(z_1,z_2) \equiv E_o^2(z_1) - E_o^2(z_2),$$

where z_1 and z_2 are two depths. Then s is the solution of

$$s^2 - 3\left[1 - s\left(\frac{a_1 - a_2 s}{a_3 - a_4 s}\right)\right]^2 \frac{\Delta E^2(z_1,z_2)}{\Delta E_o^2(z_1,z_2)} = 0 \tag{10.14}$$

that lies in the interval $0 \le s \le 1$. Note from Eq. (10.13) that $s \to 0$ as $a \to 0$, and $s \to 1$ as $b \to 0$. Here a_1, ..., a_4 are constants that depend on the

scattering phase function, but only weakly. For the Petzold turbid-harbor $\tilde{\beta}$ of Fig. 3.13 and Table 3.10,

$$\begin{aligned} a_1 &= 0.30633 \qquad a_2 = -0.32405 \\ a_3 &= 6.2114 \qquad a_4 = 4.5767 . \end{aligned} \tag{10.15}$$

Thus all of the quantities in Eq. (10.14), except s, are known if the shape of the phase function is assumed and the irradiance quartet is measured at two depths. For most natural waters, the a's given in Eq. (10.15) should be acceptably close to the actual, but unknown, a's. A root-finding algorithm must be used to find s. If a value for g is assumed, then b/a can be obtained from Eq. (10.13) using the recovered value of s. For the Petzold $\tilde{\beta}$ corresponding Eq. (10.15), $g = 0.933$. Numerical tests of the McCormick-Rinaldi algorithm show that s is recovered to within 1% of its true values for depths greater than 14 m when $\omega_o \leq 0.84$, if there are negligible errors in the measured irradiances. The recovered s becomes less accurate near the sea surface, if $\omega_o > 0.84$, and if there are random errors in the measured irradiances.

Recovery of internal sources

In the algorithms discussed above, light from internal sources such as bioluminescence or fluorescence is a source of error in the recovered IOP's. However, one person's noise is another person's signal. Sunlight-induced fluorescence can contribute significantly to underwater light fields at certain wavelengths, as can night-time bioluminescence. There is therefore considerable interest in developing ways to determine the location and strength of naturally occurring internal sources.

A recent series of papers culminating in Tao, *et al*. (1994; see references therein) has presented algorithms for the recovery of internal source locations and strengths using only *in situ* irradiance measurements. A radiometer detects the total amount of light entering it. The inherent difficulty in this problem thus lies in separating the contribution to the measured total light field made by the internal source from the contribution made by external sources such as the sun or moon.

The Tao, *et al*. algorithm is complicated, so we shall forego presenting the equations. However, the essence of the method is as follows. It is assumed that the irradiance quartet is measured, and that the phase function of the water is known. Since $\tilde{\beta}$ is not measured in practice, it reasonably can be assumed that a particle-like (Petzold) phase function describes the water body. The RTE is integrated over direction to develop

a series of equations governing certain moments of the radiance, $E_n(z)$, $n = 0$, 1, ... These moments are defined by

$$E_n(z) \equiv \int_{-1}^{1} P_n(\mu) \left[\int_{0}^{\pi} L(z;\mu,\phi)\, d\phi \right] d\mu ,$$

where $P_n(\mu)$ is the Legendre polynomial of order n. Note that $E_0(z)$ is just the scalar irradiance, and that $E_1(z)$ is the net irradiance $E_d(z)$ - $E_u(z)$. The first equation so obtained is just the divergence law (5.35), i.e. Gershun's law including the internal source term. The second equation relates the depth derivative of $\mathscr{E}_1 \equiv E_d + E_u$ to $E_{od} - E_{ou}$ and to E_n, $n \geq 1$. Subsequent equations involve the depth derivatives of higher-order E_n's ($n > 1$). Since the higher-order E_n's cannot be determined from the measured irradiance quartet, the infinite sequence of equations is terminated at three by relating the higher-order E_n's to the asymptotic radiance distribution determined from the assumed $\tilde{\beta}$. It is also assumed that the source strength varies linearly between the depths z_i where the irradiance quartet is measured. Thus $E_o^S(z) = Q_c(i) + Q_\ell(i)z$ for $z_i \leq z \leq z_{i+1}$, where E_o^S is the source term seen in the divergence law (5.35).

Several algorithms based on the above ideas have been tested numerically. The most successful one is an implicit scheme that minimizes a nonlinear functional involving the measured irradiances, the absorption coefficient, and the two parameters Q_c and Q_ℓ defining the internal source. Initial numerical tests of this algorithm are encouraging. The absorption coefficient a and the depth profile (location and strength) of the internal source are accurately recovered at depths below about 10 m. The presence of realistic amounts of random noise in the measured irradiances does not significantly degrade the algorithm's ability to recover the internal source.

10.4 Inversions Based on the Plane Irradiances

In spite of its utility, the full irradiance quartet is seldom measured. This is in part because of the difficulty of measuring E_{od} and E_{ou}; and in part because the researchers making the measurements often are interested in just K_d or R values, for example, which can be obtained from plane irradiances only. We are consequently led to investigate how much information can be extracted from E_d and E_u alone.

We first recall from Section 5.12 the various relations between K_d, R, a, b, and b_b. For example, Eq. (5.79) relates $\bar{K}_d$ to a and b/a, where $\bar{K}_d$ is the average of $K_d(z)$ over the euphotic zone. Kirk (1984) gives a similar

relation for K_{10}, the value of K_d at the depth z_{10} where E_d has decreased to 10% of its surface value:

$$K_{10} = \frac{a}{\mu_{sw}}\left[1 + (0.473\mu_{sw} - 0.218)\frac{b}{a}\right]^{1/2}. \qquad (10.16)$$

As before, μ_{sw} is the cosine of the sun's zenith angle after refraction by a level water surface. The value of K_{10} must be determined by measurements of E_d just above and just below the z_{10} depth.

Equation (10.16), if coupled with a measurement of beam attenuation c and the observation that $b/a = c/a - 1$, gives a quadratic equation for a:

$$(1.218 - 0.473\mu_{sw})a^2 + \left[(0.473\mu_{sw} - 0.218)c\right]a - K_{10}^2\mu_{sw}^2 = 0. \qquad (10.17)$$

The positive root for a then yields $b = c - a$. The backscatter coefficient then can be determined from Eq. (5.75):

$$b_b = \frac{a\,R(0)}{0.975 - 0.629\mu_{sw}}, \qquad (10.18)$$

where $R(0) = E_u(z{=}0)/E_d(z{=}0)$. Finally, we note that Kirk based the numerical simulations leading to Eqs. (10.16)-(10.18) on the assumption that the Petzold turbid-harbor phase function of Fig. 3.13 is appropriate.

Various researchers have used the above, or similar, relations to recover absorption and scattering values. For example, Weidemann and Bannister (1986; see other reference therein) used measurements of E_d and E_u to compute R and K_{net} (the diffuse attenuation coefficient for $E_d - E_u$) at the 10% irradiance level, z_{10}. They obtained $\bar{\mu}_{10}$ from R_{10} using a numerically generated relation between $\bar{\mu}_{10}$ and K_{10} given in Kirk (1981). They then obtained a from Gershun's law in the form of Eq. (5.69):

$$a_{10} = \bar{\mu}_{10}E_{net,10}.$$

Substituting this value of a into Eq. (10.16) gave b/a at z_{10}, from which b_{10} was obtained by $b_{10} = a_{10}\times(b/a)_{10}$.

Weidemann and Bannister also used standard laboratory techniques of filtration, centrifugation, and spectrophotometry to determine the individual contributions to absorption by pure water, dissolved organic substances (yellow matter), and particles (both chlorophyll-bearing and detrital). The optically obtained, total a was in reasonable agreement with the sum of the component contributions obtained by the laboratory

techniques. The data taken by Weidemann and Bannister were from a eutrophic, freshwater lake with chlorophyll concentrations of 15-35 mg m^{-3}. The 10% irradiance level was usually between 2.0 and 2.5 m.

Gordon's inversion of K_d and R

Gordon (1991) used numerical simulations for a wide range of oceanic conditions to develop explicit algorithms for retrieving a, b and b_b from measurements of the plane irradiances E_d and E_u, and of the beam attenuation coefficient c. Let K and R denote the respective values of $K_d(z)$ and $R(z)$ measured just below the sea surface. The measured value of K in first normalized in the manner described in detail in Section 3.2, namely by dividing K by a certain downwelling distribution function D_o. We explained in Section 3.2 how to estimate D_o from field measurements. The normalized quantity K/D_o corresponds closely to the value of K that would be measured with the sun at the zenith, with a level water surface, and with the atmosphere removed (i.e., with a black sky).

Next let $\tilde{b}_f \equiv b_f/b$ be the probability of forward scattering for the (unknown) scattering phase function $\tilde{\beta}$; b_f is the forward scattering coefficient defined by Eq. (3.6a).

Gordon first shows that the quantity $1 - \omega_o \tilde{b}_f$ can be expanded as

$$1 - \omega_o \tilde{b}_f = \sum_{n=1}^{3} k_n \left(\frac{K}{cD_o} \right)^n , \tag{10.19}$$

where the expansion coefficients are

$$k_1 = 0.89670, \quad k_2 = 0.20271, \quad k_3 = -0.13506 .$$

This expansion recovers $\omega_o \tilde{b}_f = b_f/c$ to about 1% accuracy.

Gordon next shows that

$$\frac{b_b}{K/D_o} = \sum_{n=1}^{3} r_n [\, R(1) \,]^n , \tag{10.20}$$

where the expansion coefficients are

$$r_1 = 2.8264, \quad r_2 = -3.8947, \quad r_3 = -36.232.$$

Here $R(1) \equiv R(D_o{=}1)$ is the irradiance reflectance that would be measured in the zenith-sun, level-surface, no-atmosphere case (the only case for which $D_o = 1$). The value of $R(1)$ must be determined by extrapolation from

values of $R(D_o)$ made for two or more D_o values. For example, R can be measured at several different solar zenith angles θ_s during the course of a day; each θ_s value gives a different D_o value. The relation between $R(D_o)$ and D_o is linear for a given scattering phase function. The estimated values of $R(1)$ and the measured K and D_o values yield b_b from Eq. (10.20). This estimate of b_b is available even if c is not measured.

If c is also measured, then a and b can be determined as follows. The value of b_b obtained from Eq. (10.20) gives us

$$\frac{b_b}{K/D_o} = \frac{\omega_o \tilde{b}_b}{K/(cD_o)},$$

so that $\omega_o \tilde{b}_b$ is known. Since $\tilde{b}_f + \tilde{b}_b = 1$, we can determine ω_o from

$$\omega_o = \omega_o \tilde{b}_f + \omega_o \tilde{b}_b,$$

after obtaining $\omega_o \tilde{b}_f$ from Eq. (10.19). We now get b from $b = c\omega_o$, and a from $a = c - b$.

Gordon estimates (based on numerical simulations) that his algorithm will recover a and b to better than 1% accuracy, and b_b to better than 10%. It should be noted that this algorithm requires no assumptions about the shape of the scattering phase function. The only irradiance measurements needed are E_d and E_u just below the sea surface, and E_d just above the surface (in order to estimate D_o). Gordon also shows how the phase function $\tilde{\beta}(\psi)$ can be estimated over a limited range of scattering angles, typically $60° \le \psi \le 150°$. However, the recovery of the phase function is not as satisfactory as is the recovery of a, b, and b_b.

Detection of inelastic scattering

Numerical simulations by Ge, *et al*. (1993) show that high-spectral-resolution measurements of Fraunhofer lines can be used to determine the contribution of inelastically scattered light to the total underwater light field. Recall from Fig. 1.1 that the Fraunhofer absorption lines are very narrow (~0.1 nm) bands where there is relatively little (~20% of background) solar irradiance.

Their underlying idea is simple. Suppose that there are no inelastic scattering processes (such as Raman scattering or fluorescence) contributing to the light field near some wavelength λ, where there is a Fraunhofer line. Then the *line depth* η of the Fraunhofer line will remain unchanged with geometric depth z in the water. Recall from the discussion of Fig. 1.1 that

the line depth is defined as the ratio of the irradiance at the deepest part of the Fraunhofer line to the irradiance of the background just outside the line. For the line at $\lambda = 486.13$ nm mentioned in the discussion of Fig. 1.1, $\eta = 0.2$. However, if there are broadband (relative to the width of the Fraunhofer line) inelastic contributions to the light field near λ, then the line depth η will decrease with depth in the water as the solar contribution decreases and the total light field becomes dominated by inelastically scattered light, which is nearly constant over wavelength intervals of a few nanometers. A line depth of $\eta = 1$ means that the solar light, along with its Fraunhofer line, has completely disappeared leaving only light inelastically scattered from the wavelengths. Using measured values of η at the surface ($z = 0$) and at depth, it is then possible to separate the total irradiance into elastically and inelastically scattered parts. The numerical simulations in Ge, *et al*. (1993) indicate that this novel use of high-resolution spectral irradiance measurements may provide a new way of detecting sunlight-induced fluorescence by dissolved organic substances (which fluoresce at all visible wavelengths). Similar calculations have been performed by Kattawar and Xu (1992).

10.5 Remote Sensing

The preceding sections of this chapter have discussed the inversion of radiometric measurements made within the water. We now consider the use of measurements made remotely from aircraft or satellites as a way of obtaining information about the IOP's or constituents of natural waters.

Oceanic remote sensing using electromagnetic signals is commonly performed from the near UV to various radar bands, whose wavelengths range from ~1 cm to ~1 m.

This remote sensing can be *active* or *passive*. *Active remote sensing* means that a signal of known characteristics is sent from the sensor platform – an aircraft or satellite – to the ocean, and the return signal is then detected after a short time delay determined by the distance from the platform to the ocean and by the speed of light. An example of active remote sensing at visible wavelengths is the use of laser-induced fluorescence to detect chlorophyll, yellow matter, or pollutants. In laser fluorosensing, a pulse of UV light is sent to the ocean surface, and the spectral character and strength of the induced fluorescence at UV and visible wavelengths gives information about the location, type and concentration of fluorescing substances in the water body. Laser fluorosensing is discussed, for example, in Measures (1992).

In *passive remote sensing* we simply observe the electromagnetic radiation that is naturally emitted or reflected by the water body. One example at visible wavelengths would be the night-time detection of bioluminescence from aircraft. Another example is the detection of sunlight that has been backscattered by the water.

The full range of these remote sensing methods and their applications can be seen in the books by Saltzman (1985), Robinson (1985), and Stewart (1985). In this section we shall discuss a small but very important subset of remote sensing: the use of "ocean color" to obtain information about natural water bodies.

Ocean color

As we saw in Chapter 2, the color of a water body can be computed if a spectral radiometric quantity is measured over the visible wavelengths. In practice this is seldom done. Spectral signals usually are measured at only a few selected wavelengths, and other forms of information than the color itself can be obtained from such data. The term "ocean color" is therefore loosely used to mean radiometric data at two or more visible wavelengths, from which useful information about water bodies can be extracted.

Conceptually, ocean-color remote sensing is simple. Sunlight, whose spectral properties are known, enters a natural water body. The spectral character of the sunlight is then altered, depending on the absorption and scattering properties of the water body, which of course depend on the types and concentrations of the various constituents of the particular water body. Part of the altered sunlight eventually makes its way back out of the water, and can be detected from an aircraft or satellite. If we know how different substances spectrally alter sunlight, for example by wavelength-dependent absorption or by fluorescence, then we can hope to deduce from the altered sunlight what substances must have been present in the water, and in what concentrations.

The *water-leaving radiance*, which is commonly denoted by L_w, is the upwelling radiance measured in the air just above the water surface. In our notation, then,

$$L_w(\theta,\phi;\lambda) \equiv L^-(z=a;\theta,\phi;\lambda) ,$$

where $\pi/2 < \theta \leq \pi$ in our coordinate system. A sensor looking straight down at the water surface sees the zenith radiance heading straight upward,

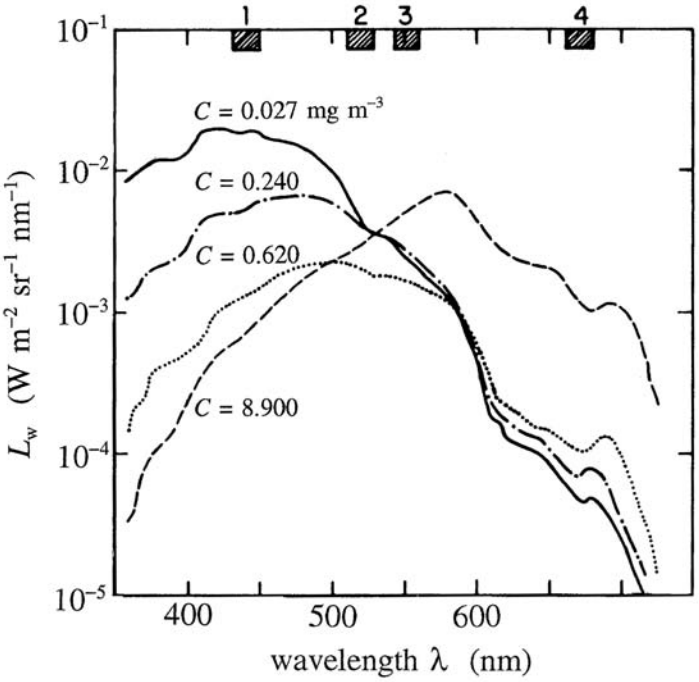

Fig. 10.1. Water-leaving radiances L_w as a function of wavelength for four chlorophyll concentrations C, in case 1 waters. The shaded regions labeled 1-4 indicate the detector bandwidths of the CZCS sensor. [redrawn from Gordon, *et al.*, (1985), by permission]

i.e., photons traveling in the $\theta = \pi$ direction. This special case of $L_w(\theta=\pi)$ is sometimes called the nadir-viewing radiance.

Figure 10.1 shows the water-leaving radiance for several concentrations of chlorophyll *a* in case 1 waters. We could compute the color associated with these $L_w(\lambda)$'s by using the formulas of Chapter 2. Clearly, the color shifts from blue to green as the chlorophyll concentration C increases. By plotting the color on a CIE chromaticity diagram for different values of C, we could determine the path followed across the diagram as C increases. If we then measured $L_w(\lambda)$ from a water body with an unknown C value, we could compute the color, compare it with the colors for known C values, and determine the value of C that most closely corresponds to the color of the water body in question. In so doing, we would have estimated the chlorophyll concentration of the water body using only the remotely sensed spectral radiance.

However, such complete spectral information is seldom available. The four shaded regions at the top of Fig. 10.1 show the bandwidths of the four visible-wavelength channels of the Coastal Zone Color Scanner (CZCS). CZCS was a satellite ocean-color sensor, which was in operation from 1978 to 1986. These four bands are centered at $\lambda_1 = 443$ nm, $\lambda_2 = 520$ nm, $\lambda_3 = 550$ nm, and $\lambda_4 = 670$ nm. We can see from the figure that *the ratios of L_w in two different sensor bands vary in a systematic way with chlorophyll concentration. This observation is the key to ocean color remote sensing as it is commonly practiced.*

Let $R(i,j)$ denote the ratio

$$R(i,j) \equiv \frac{L_w(\lambda_i)}{L_w(\lambda_j)}, \tag{10.21}$$

where $i, j = 1, 2, 3, 4$ for the CZCS. Figure 10.2 shows the value of the chlorophyll concentration C as a function of $R(1,3) = L_w(\lambda_1{=}443)/L_w(\lambda_3{=}550)$, for case 1 water. The correlation between $\log C$ and $\log R(1,3)$ means that *we can estimate C from radiance remotely measured at only two wavelengths* (on the assumption that we are in case 1 water).

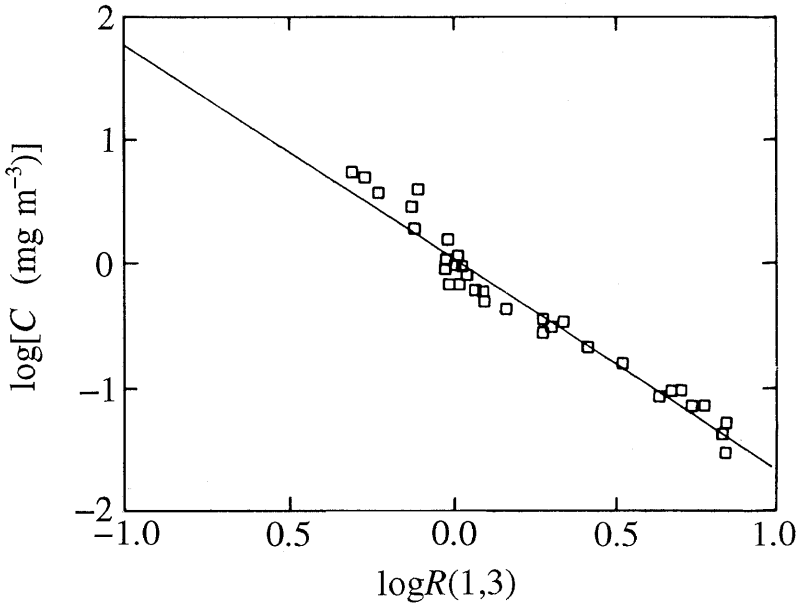

Fig. 10.2. Chlorophyll concentration C as a function of the water-leaving radiance ratio $R(1,3)$, for case 1 waters. [reproduced from Gordon, *et al.* (1983), by permission]

The roughly linear dependence of log$C$ on log$R$(1,3) seen in Fig. 10.2 suggests a relation of the form

$$\log C = A(i,j) + B(i,j) \log R(i,j) , \tag{10.22}$$

where $A(i,j)$ and $B(i,j)$ are coefficients that depend on the particular sensor wavelengths λ_i and λ_j used in computing the radiance ratio $R(i,j)$. The solid line in Fig. 10.2 is the least-squares best-fit curve of the form (10.22).

Relationships like Eq. (10.22) can be used to retrieve other quantities as well. For example, Fig. 10.3 shows the dependence of $K_d(\lambda=490)$ on the R(1,3) ratio. The solid curve is given by

$$K_d(490) = K_{d,w}(490) + 0.0883 R(1,3)^{-1.491} , \tag{10.23}$$

which has the form of Eq. (10.22) if logarithms are taken. Here, $K_{d,w}(490)$ is the downwelling diffuse attenuation coefficient of pure water; $K_{d,w}(490)$ = 0.021 m^{-1} from Table 3.5.

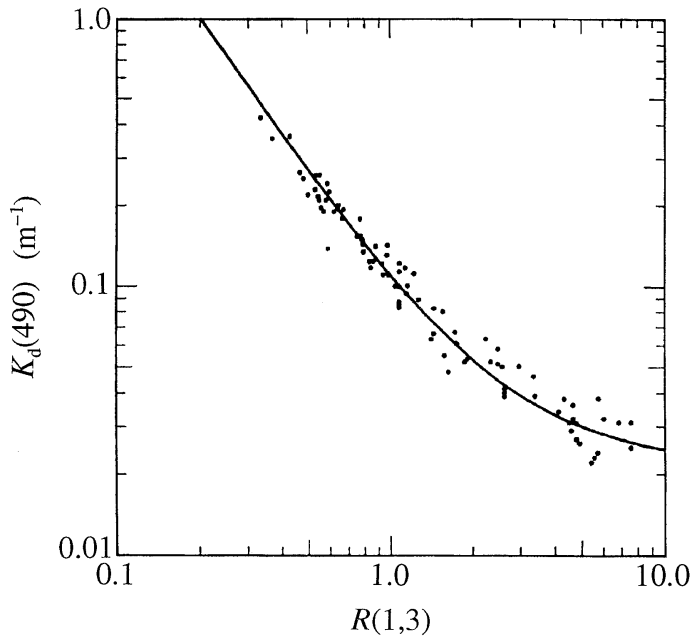

Fig. 10.3. K_d at λ = 490 nm as a function of the water-leaving radiance ratio R(1,3). The solid curve is given by Eq. (10.23). [redrawn from Austin and Petzold (1981), by permission]

Complications

As might be suspected, the actual use of remotely sensed radiances to recover chlorophyll concentrations is more complicated than indicated in the above discussion. The major difficulty in the use of data obtained by satellites arises because of the intervening atmosphere. The radiance detected at the satellite includes not just the water leaving radiance, which carries the information about the water body. The detected radiance also includes contributions by sky radiance reflected toward the sensor by the sea surface and, most importantly, by solar radiance scattered toward the sensor by atmospheric gases and aerosols. In practice, the water-leaving radiance accounts for less than 10% of the total radiance detected at the satellite.

The confounding effects of the atmospheric contribution can be removed if the optical properties of the atmosphere are known. In essence, we must perform a radiative transfer calculation for the atmosphere in order to predict how much of the solar beam will be scattered towards the sensor and transmitted through the atmosphere to it. This calculation depends on the relative position of the sun and sensor, as well as on the nature and vertical distribution of atmospheric aerosols. Unfortunately, atmospheric aerosols are quite variable in kind, concentration, and distribution. The atmospheric correction calculations therefore always involve a certain amount of educated guessing. In any case, after the atmospheric (and sea surface) effects have been predicted, the associated radiance is subtracted from the measured radiance in order to obtain an estimate of the actual water-leaving radiance. Details of the rather complicated atmospheric-correction process are given in Gordon and Morel (1983) and in Gordon, *et al.* (1988).

The paper by Gordon, *et al.* (1988) also develops a more sophisticated model than Eq. (10.22) for the retrieval of C from $R(i,j)$. This more recent inversion algorithm includes the effect of yellow matter derived from phytoplankton, and gives a nonlinear relation between $\log C$ and $\log R(1,3)$, but still is applicable only to case 1 waters.

Remote sensing of case 2 waters is much more complicated because we must be able to separate the effects of chlorophyll from the effects of mineral particles or high concentrations of terrestrially derived yellow matter. This separation can be partially achieved by the addition of carefully chosen wavelength bands. For example, the SeaWiFS (Sea-viewing Wide-Field-of-view Sensor, scheduled for launch in 1994) ocean color sensor will have a band centered at 412 nm. This band will help distinguish yellow matter, which has high absorption at 412 nm [recall Eq.

(3.25)], from chlorophyll, whose absorption decreases below ~440 nm (recall Fig. 3.7).

The coming availability of high-spectral-resolution data opens the door to other kinds of remote-sensing algorithms. For example, preliminary work (C.O. Davis, personal communication) indicates that the wavelength derivative $dL_w/d\lambda$ evaluated at λ = 570 nm can be used to distinguish suspended sediments (or bottom reflectance in shallow waters) from biological particles. Likewise $dL_w/d\lambda$ at λ = 710 nm can be used to identify kelp beds. Such derivatives cannot be estimated if only a few wavelength bands are measured. The development of remote-sensing inversion algorithms for use in case 2 waters scarcely has begun. As with other facets of the hydrologic optics of such waters, the remote sensing of case 2 waters will provide challenging research problems for a generation of scientists.

Remote-sensing reflectance

We have now encountered the essential ideas upon which ocean color remote sensing rests. However, we cannot end this section without discussing the *remote-sensing reflectance* R_{rs}, which was defined in Eq. (3.18) as

$$R_{rs}(\hat{\xi}) \equiv \frac{L_w(z=a;\hat{\xi})}{E_d(z=a)} \qquad (\text{sr}^{-1}) . \tag{10.24}$$

We can now understand the utility of R_{rs}. The downwelling irradiance onto the sea surface, $E_d(a)$, can be considered as known; $E_d(a)$ is usually obtained from a simple atmospheric radiative transfer model such as that of Gregg and Carder (1990). R_{rs} therefore provides the connection between the known input to the water body and its output, which is the water-leaving radiance. This connection warrants further investigation.

Let us recall how $E_d(a)$ gets into the water, and then how upwelling radiance gets out of the water. First, from the interaction principle of Eq. (4.6), we have

$$E_d(w) = E_u(w)\, r(w,a) + E_d(a)\, t(a,w) ,$$

or

$$E_d(a) = \frac{E_d(w) - E_u(w)\, r(w,a)}{t(a,w)} . \tag{10.25}$$

As always, $t(a,w) = 1 - r(a,w)$. The *irradiance* reflectances $r(a,w)$ and

$r(w,a)$ were studied extensively in Chapter 4. Next, consider the upwelling radiance just beneath the surface, $L^-(w;\hat{\xi}')$, $\hat{\xi}' \in \Xi_u$, being transmitted through the surface to give the water-leaving radiance $L_w(a;\hat{\xi}) = L^-(a;\hat{\xi})$, $\hat{\xi} \in \Xi_u$. The n^2 law for radiance, Eq. (4.21c), relates these two quantities:

$$L_w(a;\hat{\xi}) = \frac{t_F(w,a;\hat{\xi}'\rightarrow\hat{\xi})}{n_w^2} L^-(w;\hat{\xi}') . \tag{10.26}$$

Here $n_w \approx 1.34$ is the index of refraction of the water, and $t_F(w,a;\hat{\xi}'\rightarrow\hat{\xi})$ is the Fresnel *radiance* transmittance from water to air ($t_F = 1 - r_F$, as discussed in Chapter 4.

Substituting Eqs. (10.25) and 10.26) into (10.24) gives

$$R_{rs}(\hat{\xi}) = \frac{t(w,a;\hat{\xi}'\rightarrow\hat{\xi})\, t(a,w)}{n_w^2} \frac{L^-(w;\hat{\xi}')}{E_d(w) - E_u(w)\, r(w,a)} .$$

This equation can be rewritten as

$$R_{rs}(\hat{\xi}) = \frac{t(w,a;\hat{\xi}'\rightarrow\hat{\xi})\, t(a,w)}{n_w^2 [\,1 - R(w)\, r(w,a)\,]} \frac{R(w)}{Q(w;\hat{\xi}')} , \tag{10.27}$$

where

$$R(w) \equiv \frac{E_u(w)}{E_d(w)} ,$$

and

$$Q(w;\hat{\xi}') \equiv \frac{E_u(w)}{L^-(w;\hat{\xi}')} \qquad (\text{sr}) . \tag{10.28}$$

Equation (10.27) is exact. It is often encountered in the literature in an approximate form valid for many remote sensing situations. Let us consider only the case of $\hat{\xi}'$ and $\hat{\xi}$ nearly normal to the mean sea surface. Then $t_F(w,a;\hat{\xi}'\rightarrow\hat{\xi}) \approx 1 - r_F(\hat{\xi}'\cdot\hat{n}\approx 1) \approx 0.98$, where $r_F(\hat{\xi}'\cdot\hat{n})$ is the Fresnel reflectance of a level surface, as seen in Fig. 4.3. Now from Figs. 4.11 and 4.16, we see that $r(a,w) < 0.07$ for the sun within 60° of the zenith in a clear sky, or for overcast skies. Typically, $t(a,w) = 1 - r(a,w) \approx 0.96$. Likewise, from Fig. 4.17, $r(w,a) < 0.7$ for diffuse upwelling light fields. The irradiance reflectance R is almost always less than 0.1 in case 1 waters. Thus, Eq. (10.27) can be approximated by

$$R_{rs} \approx 0.54 \frac{R}{Q} \qquad (\text{sr}^{-1}) . \tag{10.28}$$

The ratio R/Q can be connected with the IOP's of a water body. For example, Gordon, *et al*. (1988) show that for case 1 waters,

$$\frac{R}{Q} \approx 0.095 \frac{b_b}{a + b_b}, \tag{10.30}$$

and that

$$\frac{R}{Q} \approx 0.11 \frac{b_b}{K_d}. \tag{10.31}$$

The approximation (10.31) is accurate to better than 20%.

Suppose, for example, that we determine R_{rs} from a modeled value of $E_d(a)$ and a remotely sensed value of L_w, and that we remotely determine K_d as in Eq. (10.23). Then we can combine Eqs. (10.29) and (10.31) to obtain an estimate of the IOP b_b, or of the absorption a if we then employ Eq. (10.30).

Zaneveld (1989) has pointed out that similar formulas based on *in situ* measurements of $L^-(z;\theta=180)/E_{od}(z)$ can be used to recover b_b after a is determined via Gershun's law.

The remote sensing reflectance is of such great utility that commercial instrument packages often include sensors for the simultaneous measurement of $L^-(z;\theta=180;\lambda)$ and $E_d(z;\lambda)$ at the wavelengths of interest for remote sensing. However, the user of convenient formulas like (10.29)-(10.31) must keep in mind that they are approximations based on a certain geometry, namely $\hat{\xi}'$ and $\hat{\xi}$ pointing toward the zenith, and on the assumption of case 1 water. If our remote sensing radiometer is pointed away from the nadir direction, we must return to the exact formula (10.27) and take into account the bidirectional dependence of $t_F(w,a;\hat{\xi}'\rightarrow\hat{\xi})$ and the directional dependence of $Q(w;\hat{\xi}')$. Algorithms with this level of sophistication have seldom been used in ocean color remote sensing studies, in part because the needed information has not been available.

Morel and Gentili (1993) have recently studied the dependence of Q, an AOP, on direction, wavelength, water IOP's, and sky conditions. They found that Q values generally range from 3 to 6, with the low values occurring in clear waters at blue wavelengths, and with the high values occurring at higher chlorophyll concentrations and red wavelengths, in case 1 waters. Detailed studies such as Morel's and Gentili's, along with computations of radiance transmittances for sea various states and incident and transmitted directions, as illustrated in Section 4.8, form the basis for improved remote sensing algorithms.

Gordon and Morel (1983) and Gordon, *et al*. (1985) are excellent references on ocean color remote sensing. The conference proceedings by Gower (1987) show the incredible variety of oceanographic studies that have employed data from the Coastal Zone Color Scanner.

10.6 Problems

10.1 The irradiance data shown in Table 10.1 were taken (actually, numerically simulated using the model developed in Chapter 8) under the following conditions:

clear sky
solar zenith angle: $\theta_s = 38°$
solar direct-beam irradiance: $E_d(\text{sun}) = 0.569$ W m^{-2} nm^{-}
diffuse sky irradiance: $E_d(\text{sky}) = 0.100$ W m^{-2} nm^{-1}
wind speed: $U = 7.2$ m s^{-1}
well mixed water
chlorophyll concentration: $C = 0.5$ mg m^{-3}
wavelength: $\lambda = 500$ nm
beam attenuation coefficient: $c = 0.274$ m^{-1}.

(a) Using the measured irradiance data, estimate a, b, and b_b as many ways as possible.
(b) Do the values from (a) agree with the values predicted by the bio-optical models of Chapter 3?

10.2. Using the data of Table 10.1, compute the values of R, R_{rs}, and Q at z = a, 1 m, 5 m, and 100 m.

10.3. What is the value of Q if the upwelling radiance distribution $L^{-}(\hat{\boldsymbol{\xi}})$ is isotropic?

10.4. Show that the absorption a can be obtained from b_b and R_{rs} by

$$a = b_b \left(\frac{0.051}{R_{rs}} - 1 \right).$$

This result gives a negative absorption if $R_{rs} > 0.051$. However, in extremely turbid case 2 waters, R_{rs} can be greater than 0.051. What is wrong with the above formula for a?

Table 10.1. Spectral irradiance and zenith (nadir-looking) radiance values for use in problems 10.1 and 10.2. All irradiances have units of W m^{-2} nm^{-1} and L^- has units of W m^{-2} sr^{-1} nm^{-1}; 5.879−2 means 5.879×10^{-2}, etc.

z (m)	E_{ou}	E_{od}	E_u	E_d	$L^-(\theta=\pi)$
air	5.879−2	9.000−1	2.726−2	6.691−1	5.647−3
0	4.684−2	7.800−1	1.888−2	6.607−1	3.952−3
1	4.557−2	7.398−1	1.804−2	6.147−1	3.705−3
2	4.385−2	6.980−1	1.713−2	5.711−1	3.464−3
5	3.767−2	5.753−1	1.433−2	4.546−1	2.800−3
10	2.735−2	4.012−1	1.014−2	3.057−1	1.915−3
20	1.280−2	1.812−1	4.644−3	1.335−1	8.501−4
30	5.605−3	7.840−2	2.018−3	5.707−2	3.657−4
40	2.397−3	3.340−2	8.607−4	2.424−2	1.556−4
50	1.017−3	1.417−2	3.651−4	1.028−2	6.602−5
60	4.309−4	6.006−3	1.547−4	4.361−3	2.801−5
70	1.827−4	2.548−3	6.562−5	1.851−3	1.189−5
100	1.399−5	1.953−4	5.028−6	1.421−4	9.122−7

10.5. An aircraft flying 100 m above the sea surface sends a 5 ns long pulse of laser light of wavelength 532 nm toward the surface. At time 7.386×10^{-7} s later, the aircraft receives a return pulse that is interpreted as a reflection off of the bottom. How deep is the water?

Hoge, *et al.* (1988) describe how a *laser bathymetry* system with the characteristics just described was used to map a scattering layer of suspended particles at a depth of ~10 m.

Next Chapter >>